Reactions of NH_2 with NO_2 and of OH with NH_2O

F. Sun, J. D. DeSain,[†] Graham Scott,[‡] P. Y. Hung, R. I. Thompson,[§] G. P. Glass,* and R. F. Curl*

Chemistry Department and Rice Quantum Institute, Rice University, Houston, Texas 77005

Received: December 22, 2000; In Final Form: April 2, 2001

The reaction system produced by 193 nm flash photolysis of a mixture of NH_3 and NO_2 has been investigated experimentally and modeled. The accepted belief that only two channels are of significance for the reaction between NH_2 and NO_2, producing (a) N_2O and H_2O and (b) NH_2O and NO, is confirmed by the absence of H_2O_2 absorption signals and the absence of early HNO, as H_2O_2 and HNO are produced by two of the possible five $NH_2 + NO_2$ channels. The fact that the OH concentration extrapolated to the flash is less than the initial NH_2 concentration indicates that the channel producing two OH molecules is not significant. HNO is observed to be produced on a slower time scale than that of the $NH_2 + NO$ reaction and is believed to be formed by the reaction of OH with NH_2O (OH is formed by the reaction of NO_2 with H produced by the flash photolysis of NH_3). NH_2O does not appear to react with NO_2 at 296 K on our time scale. Modeling of the reaction system gives a rate for the reaction between NH_2O and OH of $1.8(10) \times 10^{-10}$ cm^3 s^{-1}. An excess continued decay of OH at long times after NH_2O has virtually disappeared can be accounted for by reaction of OH with HNO with a rate in the range $(2-8) \times 10^{-1}$ cm^3 s^{-1}.

Introduction

The interest in the reaction between NH_2 and NO_2 arises primarily from the work of Glarborg et al.,[1] who proposed that this reaction produces a significant yield of NH_2O and that this species plays a key role in the thermal DeNox process[2] (i.e., the selective noncatalytic reduction of NO by ammonia). The reaction is also of some importance in the mechanism of decomposition of the solid propellant ammonium dinitramide.[3,4]

Several possible product channels of the title reaction are thermodynamically accessible.[1,5] Among these are

$$NH_2 + NO_2 \rightarrow H_2O + N_2O \quad (\Delta H = -378 \text{ kJ/mol}) \qquad (1a)$$

$$\rightarrow NH_2O + NO \quad (\Delta H = -67 \text{ kJ/mol}) \qquad (1b)$$

$$\rightarrow H_2O_2 + N_2 \quad (\Delta H = -355 \text{ kJ/mol}) \qquad (1c)$$

$$\rightarrow OH + OH + N_2 \quad (\Delta H = -140 \text{ kJ/mol}) \qquad (1d)$$

$$\rightarrow HNO + HNO \quad (\Delta H = -19 \text{ kJ/mol}) \qquad (1e)$$

On the basis of previous theoretical and experimental work, it is generally believed that the dominant product channels of the reaction are eqs 1a and 1b. An ab initio molecular orbital study[6] of the $NH_2 + NO_2$ potential energy surface concluded that both channels 1c and 1d are inaccessible because the energies of the transition states leading to them are higher than the energy of the reactants. This conclusion is supported by the observation of Glarborg et al.[1] that very little N_2 is formed at temperatures between 850 and 1350 K in the thermal reaction of NH_3 with NO_2. Reaction 1e is also thought to be unimportant because the most probable route to HNO + HNO involves at least one intermediate that is energetically inaccessible.[1]

Since 1995, several measurements of the product branching ratio into channel 1a, k_{1a}/k_1, have been made.[7−11] The results of these measurements vary between 0.14 and 0.59. However, the two most recent measurements are in relatively good agreement. In 1997, Park and Lin[10] reported the branching ratio as 0.19 ± 0.02 and determined that it did not vary significantly as the temperature was raised from 300 to 910 K. In the same year, Lindholm and Hershberger[11] obtained a branching ratio of 0.24 ± 0.04 for reaction into channel 1a. These latter authors also measured (by assuming that only channels 1a and 1b are present) a branching ratio into the $NH_2O + NO$ channel, 1b, of 0.76 ± 0.1.

Despite this agreement, several problems concerning the overall mechanism of the reaction of NH_2 with NO_2 remain. The only evidence for the dominant channel (1b) is the appearance of NO as a final product, the theoretical calculations,[6] and the chemical reasonableness of the postulated reaction. At room temperature, both Quandt and Hershberger[9] and Park and Lin[8,10] observed significantly higher concentrations of H_2O than were predicted by the assumed mechanism. Also, much of the secondary chemistry remains unexplored. In view of this, we decided to re-examine the reaction by using infrared kinetic spectroscopy.

Experimental Section

In these experiments, a mixture of NH_3 and NO_2 in the presence of excess He buffer gas is flash photolyzed at 193 nm and the time evolution of products observed by time-resolved laser-based infrared absorption spectroscopy. A schematic diagram of the apparatus is shown in Figure 1. A standard multipass ("white") infrared absorption cell was used. The IR probe beam traveled back and forth throughout this cell in the horizontal plane, while the UV photolysis beam was angled

[†] Present address: Combustion Research Facility, Sandia National Laboratories, Livermore, CA 94551-0969.

[‡] Present address: Department of Molecular and Human Genetics, Baylor College of Medicine, One Baylor Plaza, Houston, TX 77030.

[§] Present address: Department of Physics and Astronomy, University of Calgary, Calgary, Alberta T2N 1N4, Canada.

10.1021/jp004570x CCC: $20.00
Published on Web 06/06/2001

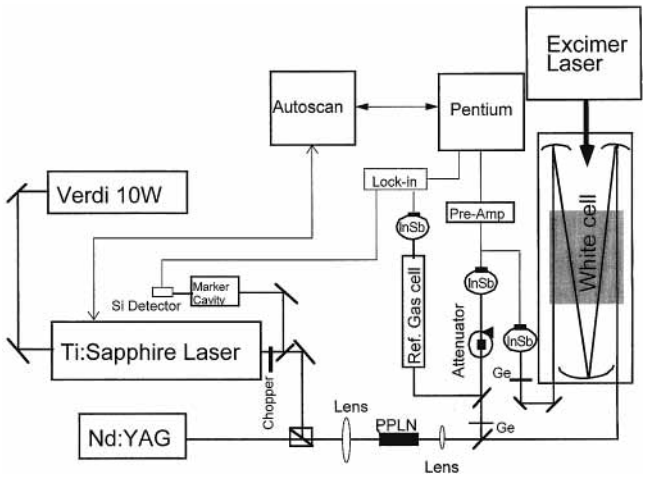

Figure 1. Infrared kinetic spectroscopy apparatus using a DFG source. A second apparatus employed in this work uses a color center laser source.

TABLE 1: Transitions, Frequencies, and Peak Infrared Absorption Cross Sections of Species Monitored

species	transition	frequency (cm^{-1})	σ_0 ($\times 10^{18}$ cm^2)
NH_3	ν_3 $s^pP_6(7)$[a]	3345.621	0.37[b]
NO_2[c]	$\nu_1 + \nu_3$ $16_{4,13} \leftarrow 15_{4,12}$ F_1	2915.854	0.61
NH_2	ν_1 $6_{4,2} \leftarrow 5_{3,3}$ F_1[d]	3428.786	0.37[b]
OH[c]	P(4,5)1+	3407.989	4.37
N_2O[c]	$2\nu_1$ R(16)	2576.5415	4.69
H_2O[c]	ν_1 $5_{41} \leftarrow 6_{34}$	3607.263	0.75
NO[c]	v 2 ← 0 P_{22}(8.5)f	3693.4792	0.087
HNO	ν_1 $5_{14} \leftarrow 5_{23}$[e]	2632.8088	1.81[f]
H_2O_2[g]	$\nu_2 + \nu_6$ $^rQ_0$	2658.7	unknown
CH_3	ν_3 $^rQ_0(2)$[h]	3154.7468	3.00[i]

[a] From ref 12. [b] From ref 13. [c] From ref 14. All ref 14 cross sections assume a line width determined by Doppler broadening. [d] From ref 15. [e] From ref 16. [f] From ref 17. [g] From ref 18. [h] From ref 19. [i] This work.

upward as it traversed the cell, so as to intersect the IR beam over the approximately 35-cm section of the cell that is shaded.

Two different tunable infrared laser sources were used in this investigation, a CW color center laser (Burleigh Instruments, FCL-20, Li:RbCl crystal, 2.6−3.2 μm), pumped by a krypton ion laser, and a newly developed laser based on difference frequency generation (DFG) in periodically poled $LiNbO_3$. The DFG apparatus is diagrammed in Figure 1; the color center laser apparatus is similar except that the DFG IR generation system is replaced by a color center laser pumped by a Kr^+ laser.

Reaction mixtures typically contained 3−10 mTorr of NH_3, 30 mTorr of NO_2, and 9 Torr of He. Under normal operating conditions, 10−15% of the ammonia in the excimer beam was dissociated by the laser pulse.

To avoid depletion of reagents and buildup of reaction products in the photolysis cell, the transit time through the cell was decreased by increasing the pumping speed and by decreasing the diameter of the glass tube forming the cell wall. This ensured that the reaction mixture was exposed to only one photolysis pulse during transit through the cell. The depletion by the first shot and the subsequent chemistry was 10−20% for NH_3 and 5−10% for NO_2, and the buildup of NO per shot was about 5−10% of the original NO_2 concentration.

Table 1 lists the identity of the species monitored during this investigation, the particular infrared transitions that were monitored,[12−19] the frequencies (cm^{-1}) of these transitions, and the peak infrared absorption cross sections (excepting H_2O_2). Infrared absorbance measurements were converted into column densities by using the equation

$$A_e = \sigma NL \tag{2}$$

where A_e is the base e absorbance, σ is the peak infrared absorption cross section, N is the species concentration in molecules/cm^3, and L is the path length. Because of the way that the infrared beams only partially overlap the excimer beam in the multipass arrangement of Figure 1, the path length, L, is not easy to calculate accurately and instead was measured in the scheme described here.

An effective value for L was obtained by measuring the recombination rate of methyl radicals and the observed CH_3 absorbance. This scheme can be outlined as follows. The reaction is

$$2CH_3 \rightarrow C_2H_6 \tag{3}$$

The concentration of CH_3 as a function of time is given by the standard second-order rate law expression.

$$[CH_3] = \frac{[CH_3]_0}{1 + 2k_3[CH_3]_0 t} \tag{4}$$

However, the absorbance given by eq 4 is measured so that the time behavior of the methyl signal is given by

$$A(t) = \frac{A_0}{1 + \kappa A_0 t} \tag{5}$$

with $\kappa = 2k_3/(\sigma_0 L)$. Thus, by measuring κ, the path length can be calculated from

$$L = \frac{2k_3}{\kappa\sigma_0} \tag{6}$$

if k_3 and σ_0 are known. Under the experimental conditions, the second-order rate constant for this reaction is[20] $k_3 = 3.7 \times 10^{-11}$ cm^3 s^{-1}. However, σ_0 for CH_3 is not known under the exact conditions of these experiments and must be measured.

The peak absorption cross section, σ_0, of the CH_3 line at 3154.7468 cm^{-1} was measured in the presence of 9 Torr of He by flash photolyzing N_2O (272 mTorr) at 193 nm in the presence of CH_4 (1.82 Torr), initiating the next series of reactions.

$$N_2O + h\nu\ (193\ nm) \rightarrow N_2 + O(^1D) \tag{7}$$

$$O(^1D) + CH_4 \rightarrow OH + CH_3 \tag{8}$$

$$2CH_3 \rightarrow C_2H_6 \tag{9}$$

$$CH_3 + OH \rightarrow \text{products} \tag{10}$$

Because $[CH_3]_0 = [OH]_0$, the CH_3 peak absorption cross section can be obtained by comparison of the CH_3 signal with the OH signal at $t = 0$, using the known Doppler cross section of OH.[14] (The 1/e half width of OH found in these experiments is 190 MHz, which is quite close to the Doppler width of 183 MHz.) To do this, frequency scans of the OH line at 3407.989 cm^{-1} and of the CH_3 line at 3154.7468 cm^{-1} at a series of points after the flash were obtained and fitted with a Gaussian profile as illustrated in Figure 2, giving both the peak intensities and the line widths. The resulting peak intensities are then plotted versus time and extrapolated to $t = 0$ as shown in Figure 3. The peak absorption cross section for CH_3 is calculated from

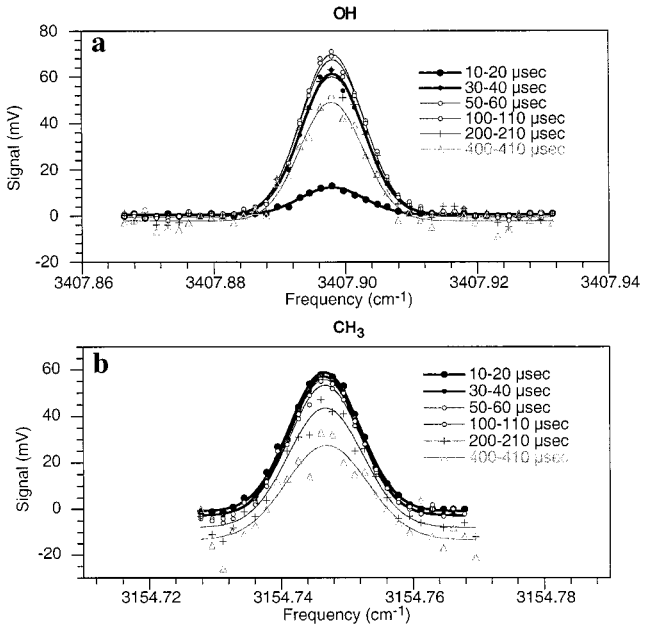

Figure 2. Frequency scans of the OH line at 3407.989 cm^{-1} and the CH_3 line at 3154.7468 cm^{-1} at various times after the photolysis flash at 193 nm of a mixture of CH_4 (1.82 Torr), N_2O (272 mTorr), NO (32 mTorr), and He (9 Torr). The times are 10−20, 30−40, 50−60, 100−110, 200−210, and 400−410 μs.

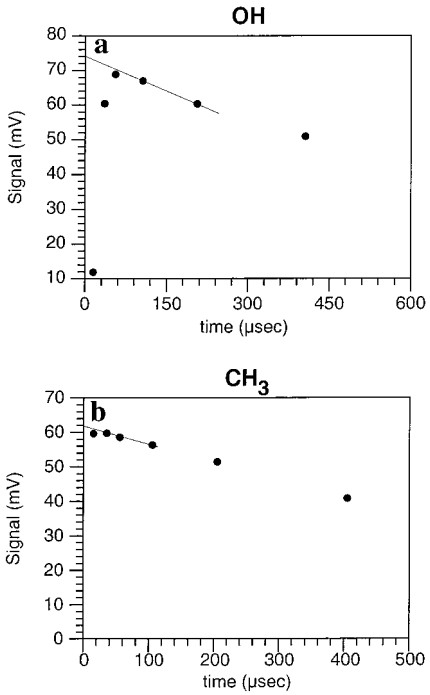

Figure 3. Extrapolations of the peak signals for OH and CH_3 from Figure 2 plotted versus time and extrapolated to $t = 0$. Total IR power signal 2.5 V for OH and 2.6 V for CH_3.

the equation

$$\sigma_0(CH_3) = \sigma_0(OH)_{Doppler} \frac{\Delta\nu(OH)_{Doppler}}{\Delta\nu(OH)_{obs}} \frac{A_0(CH_3)}{A_0(OH)} \quad (11)$$

to be 3.0×10^{-18} cm^2 at 9 Torr of He (CH_3 1/e halfwidth = 225 MHz).

Methyl radicals were produced in 9 Torr of He by the 193 nm flash photolysis of acetone (∼100 mTorr), and similar frequency scans of the CH_3 line were obtained and fitted with a Gaussian profile. The reciprocals of the peak intensities were plotted versus time to obtain κ as shown in Figure 4. The effective path length L obtained from eq 6 was 1050 cm, or 33 cm per pass in 32 passes in a 1 m white cell with partial overlap of the excimer and IR beams. An initial CH_3 concentration of about 5×10^{13} cm^{-3} was observed.

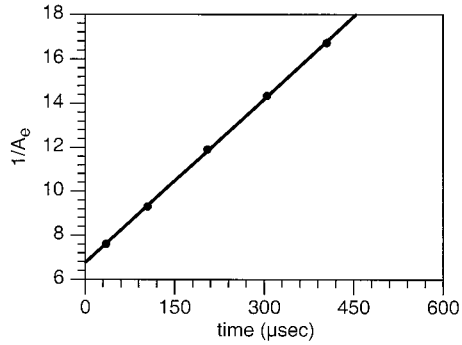

Figure 4. Reciprocals of the CH_3 absorbances plotted versus time during the decay of CH_3 by recombination. $P_{tot} = 10$ Torr.

To confirm that NH_2 is formed quantitatively by photolysis of ammonia, an initial series of experiments was performed in the absence of NO_2. NH_2 was produced with a yield of 1.0 ± 0.1 when NH_3 (∼10 mTorr) was photolyzed, and it decayed very slowly, exhibiting a half-life of about 10 ms.

Methodology

NH_2 radicals were produced by photolysis of ammonia at 193 nm using an ArF excimer laser operating at pulse energies of 50−100 mJ

$$NH_3 + h\nu \rightarrow NH_2 + H \quad (12)$$

while NO_2 is simultaneously photolyzed in a much smaller yield.

$$NO_2 + h\nu \rightarrow NO + O(^1D) \quad (13a)$$

$$\rightarrow NO + O(^3P) \quad (13b)$$

The high-resolution transient infrared absorption peaks of a number of reactants, intermediates, and products were monitored throughout the ensuing reaction using tunable infrared laser sources. A new difference frequency laser source was used that allowed all of the following species to be monitored (although NH, H_2O_2, and HONO were not in fact observed in this system): NH_3, NH_2, NH, NO_2, NO, N_2O, HNO, H_2O, OH, H_2O_2, and HONO.

The H atoms produced by the NH_3 photolysis react very rapidly (1/e = 6 μs) with NO_2 to produce NO and OH.

$$NO_2 + H \rightarrow NO + OH \quad (14)$$

The stoichiometric production of OH proved to be quite beneficial to the study, because the reaction of OH with NH_2O to produce HNO and H_2O provided indirect but powerful evidence that NH_2O is in fact being produced in high yield.

Because the 193 nm UV absorption cross section of NO_2 is relatively small ($3 \times 10^{-19}$$cm^2$)[21,22] and the absorption cross section of NH_3 at 193 nm is large (10^{-17} cm^2),[23,24] it is possible to produce $NH_2 + H$ without substantial interference from the photolysis of NO_2, even with a severalfold excess of NO_2 over NH_3. The photolysis products of NO_2, NO, $O(^3P)$, and $O(^1D)$, do not interfere significantly with the study of the $NH_2 + NO_2$ reaction. NO reacts rapidly with NH_2 but cannot compete with

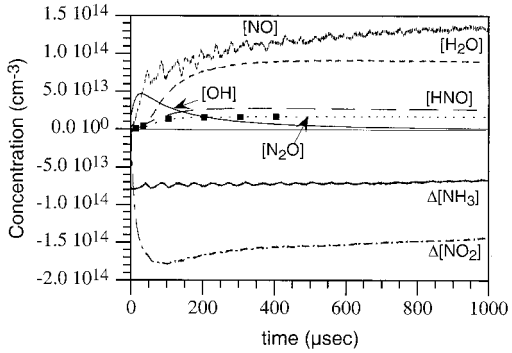

Figure 5. Time dependence of the concentrations of all the species observed. Conditions are $p_{NO_2} = 30$ mTorr, $p_{NH_3} = 10$ mTorr, and $p_{tot} = 9$ Torr using He buffer gas. Excimer energy = 90 mJ.

the large excess of NO_2 as long as flow rates are large enough and repetition rates are small enough to avoid product buildup. $O(^3P)$ reacts with NO_2, producing O_2 and NO. $O(^1D)$ also reacts in this way and, in addition, reacts with NH_3, producing NH_2 and OH.

$$O(^1D) + NH_3 \rightarrow OH + NH_2 \qquad (15)$$

This reaction has the same net products as the photolysis of NH_3.

Two kinds of data were obtained in this study: (1) time scans in which the probe frequency was tuned at or near the absorption maximum and (2) frequency scans in which the probe frequency was scanned over the line and data were acquired at six time intervals after the flash. The time scans provide more data, more rapid data collection, and better S/N for a given collection time. The frequency scans once analyzed remove any time variation in the baseline, remove any uncertainty about whether the probe is tuned to the peak of the absorption line, and simultaneously provide line widths. Each time window in a frequency scan is fitted with a Gaussian to obtain the peak absorbance and the line width. Figure 2 already illustrates this process.

Observations and Results

This reaction provides a unique opportunity for monitoring reaction products. It was possible to observe the NH_2 and NO_2 reactants, H_2O, N_2O, and NO products, and OH produced by reactions 14 and 15. In addition, HNO, which we believe is produced by a secondary reaction

$$NH_2O + OH \rightarrow HNO + H_2O \qquad (16)$$

could also be observed. Figure 5 shows the time behavior of the various species observed. It must be kept in mind that products can be produced in excited vibrational states, which have to be quenched to the ground vibrational level to be monitored. This is clearly the case for H_2O which exhibits an initial induction period.

This experiment divides roughly into two time scales. On the short time scale, reaction 14 between H and NO_2 is complete in 12 μs, and reaction 1 between NH_2 and NO_2 is about 90% complete in 100 μs. Thus, by 100 μs, H has disappeared, and the decay of NH_2 and the rise of N_2O are substantially complete. Then on a time scale of several hundred microseconds, OH decays and HNO rises through reaction 16. The time behavior of NO and H_2O is mixed. NO is produced by the photolysis of NO_2, by reactions 1b and 14, and, we believe, by the reaction sequence responsible for the slow decay of OH through the reaction

$$HNO + OH \rightarrow NO + H_2O \qquad (17)$$

Glarborg et al.[1] and Park and Lin[8] use a value for k_{17} of 6×10^{-11} cm^3 s^{-1} in their modeling. H_2O is produced by reaction 1a and by both steps of the two step secondary reaction sequence (16 and 17) responsible for the slow decay of OH. Much of this report is concerned with the interpretation and analysis of the slow processes.

The aim of this work was twofold: to obtain more direct evidence for the production of NH_2O in high yield and to obtain experimental evidence about the existence of channels 1c, 1d, and 1e, which had been found theoretically not to be open.[6] The observation of a vibrational transition of NH_2O combined with an analysis of its rotational structure would be convincing evidence for the presence of this species. However, a scan of the region 2800−3500 cm^{-1} did not reveal any spectrum that could be ascribed to NH_2O. This was somewhat surprising, as a quantum chemical calculation of the infrared intensities (and harmonic frequencies) at the B3LYP 3-311++g(2df,2pd) level indicated that the B_2 symmetry NH stretch has an intensity of 7.2 km/mol (actually, the calculation produced a nonplanar structure, but the microwave spectrum[25] analysis found a planar C_{2v} structure). This is weak, but we believe it might be detectable with our sensitivity. The A_1 symmetric NH stretch was predicted to have an intensity of 0 km/mol within reasonable error limits. The harmonic frequencies were, for A_1, 3424 cm^{-1} and, for B_2, 3556 cm^{-1}.

We made efforts to check on the existence of channels 1c, 1d, and 1e. Glarborg et al.[1] report that N_2 as determined by a nitrogen balance is less than 10% at 900 K, increasing to about 30% at 1350 K. This suggests that 1c and 1d should be negligible at room temperature. We searched for but did not observe H_2O_2. This is only mild evidence that the 1c channel is not present, because the infrared absorption cross section for the H_2O_2 line searched for is unknown (see Table 1). Because so much OH is produced so rapidly in our system, we are unable to verify independently that 1d is unimportant. Regarding channel 1e, we did observe the formation of HNO. However, HNO forms much more slowly than NH_2 disappears, actually displaying an induction period. Channel 1e is approximately 1600 cm^{-1} exoergic, and the lowest vibrational mode of HNO is at[26] 1500 cm^{-1}. This channel involves a complete rearrangement of the atoms so that there is reason to expect a statistical distribution of the reaction energy between the two HNOs produced. Thus, the slowly rising HNO signal must be from other sources (to be discussed later), and any major contribution from channel 1e is ruled out. Because the absorption cross section for the HNO line monitored is one of the largest of the species we monitored, this conclusion is on rather firm ground.

The slow decay of the OH signal and the slow rise of the HNO signal provide strong indirect evidence for the formation of large amounts of NH_2O in this system. We are convinced that these time variations arise from the rapid reaction (16) between NH_2O and OH and by a slower reaction (17) between OH and HNO. We shall present evidence that NH_2O does not react rapidly with NO_2, and it is obvious from Figure 5 that HNO does not react with NO_2 or any reaction products. By analyzing these decay profiles, rates for reactions 15 and 16 can be estimated. However, reasonably accurate OH time profiles are required in order to obtain information on these rates. First, as accurate data as possible were collected for the earlier times when reaction 16 is dominant. For this purpose,

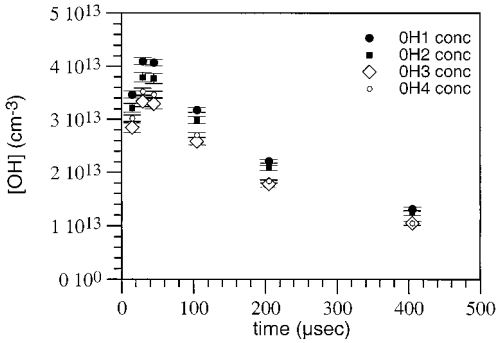

Figure 6. Concentrations as a function of time of four OH frequency scan analyses. These were obtained with $p_{NH_3} = 10$ mTorr, $p_{NO_2} = 30$ mTorr, and $p_{tot} = 9$ Torr using He buffer gas.

frequency scans were obtained and analyzed. Then a very crude estimate of the rate of reaction 17 is obtained by fitting the long time behavior of time scans.

The first step illustrates the real difficulties of rate measurements of reactions between reaction products. Data of the kind illustrated in Figure 2 must be converted into OH concentrations at each of the times given. The observed line widths (1/e HW) for all of the data to be analyzed here range from 182 to 197 MHz, and the calculated Doppler width is 183.4 MHz at 296 K. Thus, line broadening from pressure broadening and unresolved hyperfine structure is small and is neglected in converting the tabulated[16] integrated absorption line cross section into a peak cross section. Using this peak absorption cross section, the OH data from such frequency scans can be directly converted into column density and, by the use of the measured path length, into concentration. Figure 6 shows the results of such an analysis for four OH time-resolved frequency scans taken sequentially.

In this figure, there seems to be a general decrease in the OH concentration with time, as might be expected if the excimer power had drifted down or the NH_3 flow rate had drifted down. However, the decay rate of OH does not share this trend, and we shall see that the OH decay rate depends strongly upon the initial OH concentration. It seems likely that the scatter in Figure 6 is random. Therefore, the four data sets were averaged for further treatment of the time decay. On the same day that these OH data were collected, the NH_2 signal in the absence of NO_2 was also measured from three such graph sets to be 5.0×10^{13} cm^{-3}. Subsequent modeling calculations indicate that this number is about 14% too high to match the OH data. The fact that the NH_2 initial concentration is higher than that needed to model the OH data indicates that reaction channel 1d is not significant. The measurement of $[NH_2]$ is more difficult than that of [OH] because the signal is weaker, the cross sections[13] are probably less accurate, and the measurement was done in the absence of NO_2; therefore, only the OH signal measurements were used in modeling.

For modeling the kinetics in addition to the reactions given here, the reactions

$$OH + NO_2 + M \rightarrow HNO_3 + M \quad (18)$$

$$OH + NH_2 \rightarrow O + NH_3 \quad (19a)$$

$$OH + NH_2 \rightarrow H_2O + NH \quad (19b)$$

need to be included. Reaction 18 has been extensively studied. The value[27] of 4.6×10^{-13} cm^3 s^{-1} at 9 Torr of He was used for its rate (Table 2). The rate of reaction 19a is[28] 10^{-13} cm^3 s^{-1} at room temperature, which has a completely negligible effect on the OH decay. In as far as we have been able to ascertain, the rate of reaction 19b has never been measured, and we have omitted it. The OH decay is not very sensitive to this rate, as NH_2 reacts primarily with the large excess of NO_2 and disappears early in the reaction. The reaction

TABLE 2: Reactions and Rate Constants Used in the Kinetic Modeling

reaction	rate (cm^3 s^{-1})
1a. $NH_2 + NO_2 \rightarrow H_2O + N_2O$	4.80×10^{-12}
1b. $NH_2 + NO_2 \rightarrow NH_2O + NO$	1.52×10^{-11}
14. $NO_2 + H \rightarrow NO + OH$	1.20×10^{-10}
16. $NH_2O + OH \rightarrow HNO + H_2O$	1.80×10^{-10}
17. $HNO + OH \rightarrow NO + H_2O$	5.00×10^{-11}
18. $OH + NO_2 \rightarrow HNO_3$[a]	4.60×10^{-13} [a]
19a. $OH + NH_2 \rightarrow O + NH_3$	1.00×10^{-13}
20. $OH + NH_3 \rightarrow H_2O + NH_2$	1.60×10^{-13}
21. $O(^3P) + NH_2 \rightarrow HNO + H$	6.40×10^{-11}
22. $O(^3P) + NO_2 \rightarrow NO + O_2$	9.70×10^{-12}
23a. $NH_2 + NO \rightarrow H_2O + N_2$	1.44×10^{-11}
23b. $NH_2 + NO \rightarrow OH + H + N_2$	1.60×10^{-12}
24. $OH + NO \rightarrow HONO$[a]	1.50×10^{-13}

[a] The second-order rate constant of this termolecular reaction under the assumed conditions.

$$OH + NH_3 \rightarrow H_2O + NH_2 \quad (20)$$

between NH_3 and OH was included as its rate is 1.6×10^{-13} cm^3 s^{-1} at room temperature.[5]

A very minor addition to the model was the inclusion of the effect of 193 nm photolysis of NO_2. The ratio of the 193 nm absorption cross section of NO_2 to that of NH_3 is[22] 0.031. The photolysis of NO_2 produces NO and O atoms with slightly more than half of the O atoms in the $O(^1D)$ excited state, with[22] $\alpha = 0.55 \pm 0.03$.

$$NO_2 + h\nu\ (193\ nm) \rightarrow NO + \alpha O(^1D) + (1\text{-}\alpha)O(^3P) \quad (13)$$

$O(^1D)$ will disappear from the system in, at most, a few microseconds either by reaction or quenching. In contrast, $O(^3P)$ reacts away quite slowly by two reactions

$$O(^3P) + NH_2 \rightarrow HNO + H \quad (21)$$

$$O(^3P) + NO_2 \rightarrow NO + O_2 \quad (22)$$

Reactions 21 and 22 have[29,5] rate constants of $k_{21} = 6.4 \times 10^{-11}$ and $k_{22} = 1 \times 10^{-11}$ cm^3 s^{-1}. As remarked earlier, $O(^1D)$ can react rapidly with either NH_3 or NO_2. It can also be quenched by collisions with either of these gases or the He buffer gas. The extent of reaction versus quenching is difficult to estimate. Fortunately, it does not matter, as the results we obtain modeling the system assuming that all $O(^1D)$ is quenched to $O(^3P)$ are imperceptibly different from those omitting reactions 13, 21, and 22.

However, the reaction

$$NH_2 + NO \rightarrow H_2O + N_2 \quad (23a)$$

$$\rightarrow OH + H + N_2 \quad (23b)$$

with[28] $k_{23a} = 1.44 \times 10^{-11}$ and $k_{23b} = 1.6 \times 10^{-12}$ cm^3 s^{-1} does have a small but perceptible effect on the modeling. There is some controversy about whether the products of 23b should be as written above or should be $OH + HN_2$. The advantage of the choice made is that the rate constants for the reactions of H are known, while those of HN_2 are more uncertain. Because

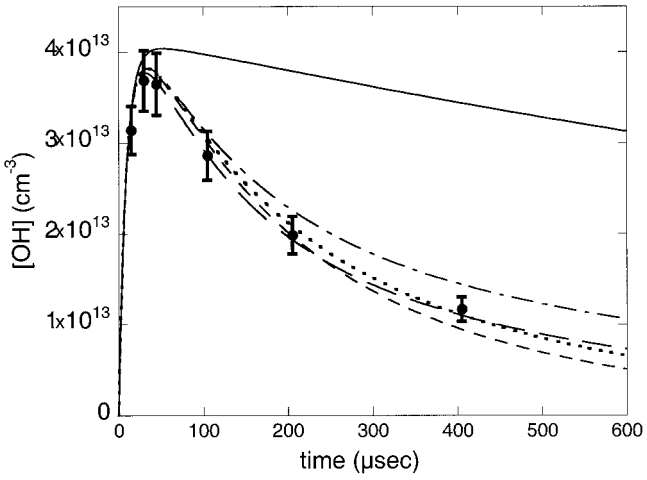

Figure 7. Average [OH] values from the data of Figure 6 are plotted as six points. The dotted curve near the points represents the expected time behavior from the model used and the fitted rate constants $k_{16} = 1.8 \times 10^{-10}$ cm^3 s^{-1} and $k_{17} = 5 \times 10^{-11}$ cm^3 s^{-1}. The upper dash−dot line corresponds to $k_{16} = 1.8 \times 10^{-10}$ cm^3 s^{-1} and $k_{17} = 0$ cm^3 s^{-1}, the lower dashed line corresponds to $k_{16} = 1.8 \times 10^{-10}$ cm^3 s^{-1} and $k_{17} = 9 \times 10^{-11}$ cm^3 s^{-1}. The long dash line corresponds to $k_{16} = 2.5 \times 10^{-10}$ cm^3 s^{-1} and $k_{17} = 2 \times 10^{-11}$ cm^3 s^{-1}. The upper solid line far from the points corresponds to $k_{16} = 0$ (and $k_{17} = 0$).

the dominant channel is 23a, we believe that the choice of products of 23a cannot affect the results. We have also included the minor reaction

$$\mathrm{OH} + \mathrm{NO} + \mathrm{M} \rightarrow \mathrm{HONO} + \mathrm{M} \qquad (24)$$

with an effective two body rate constant of 1.5×10^{-13} cm^3 s^{-1}. Anderson, Margitan, and Kaufman[30] reported the rates of reactions 18 and 24 in the same paper, finding that reaction 24 has a rate constant approximately one-third that of reaction 18. We therefore divided the rate of reaction 18 by 3 to obtain the rate of reaction 24.

Figures 7−9 show the results of modeling the OH decay by including reactions 16 and 17. Figure 7 shows the fit of the average of the OH data points shown in Figure 6. We regard these data as the most reliable, because they cannot be affected by baseline problems and because the center of the OH absorption peak is determined precisely. Figure 8 shows a fit of an OH time decay under similar conditions to Figure 7. These data were acquired several months before the data of Figure 7; the gas flow conditions should have been identical, and the excimer laser pulse energy was similar. We do not have a satisfactory explanation for the difference in the peak OH concentrations of Figures 7 and 8; possibly the alignment between the excimer and IR probe beams was different. Figure 9 shows the OH decay taken within a few minutes of that of Figure 8, but with an NH_3 concentration only about 10% of that of Figure 8. (The ratio of the two NH_3 concentrations could not be determined very precisely, because the flow controller was operating near its lower limit for the low NH_3 flow of Figure 9.) The OH concentration scale of Figures 8 and 9 could not be determined directly from the observed signal with complete reliability because of the uncertainty in setting the lasers to the OH peak. Instead, it was adjusted in the fitting process. However, Figures 8 and 9 are expected to share the same vertical scale, as the lasers were not adjusted during the data collection. Therefore, the factor used to convert absorbance to OH concentration is the same for both Figures 8 and 9.

The data of Figure 7 were used to determine k_{16} and limit k_{17}. To obtain a complete overview of the time behavior, it is

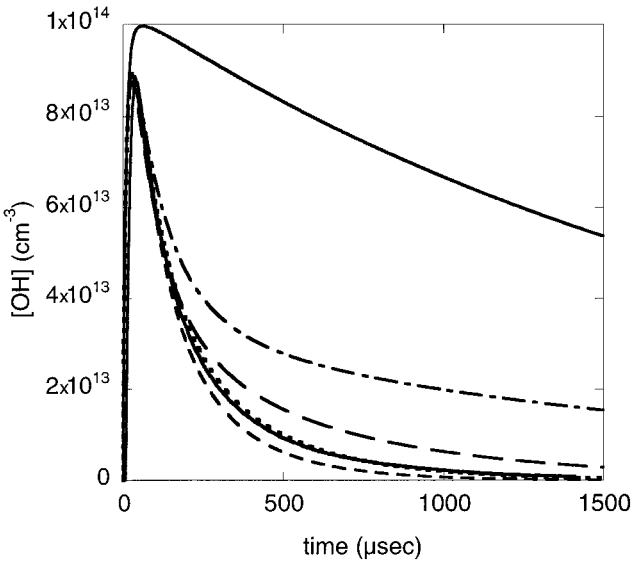

Figure 8. Time scan of [OH] concentration under the same conditions of initial concentrations. The vertical scale of this figure was adjusted to give the best fit because the probe laser may not have been set on the exact peak of the OH line. The rescaled experimental data are the heavy solid line and the dotted curve almost exactly superimposed upon it uses the fitted rate constants $k_{16} = 1.8 \times 10^{-10}$ cm^3 s^{-1} and $k_{17} = 5 \times 10^{-11}$ cm^3 s^{-1}. The upper dash−dot line corresponds to $k_{16} = 1.8 \times 10^{-10}$ cm^3 s^{-1} and $k_{17} = 0$ cm^3 s^{-1}. The long dash line directly below it corresponds to $k_{16} = 2.5 \times 10^{-10}$ cm^3 s^{-1} and $k_{17} = 2 \times 10^{-11}$ cm^3 s^{-1}. The lower dashed line corresponds to $k_{16} = 1.8 \times 10^{-10}$ cm^3 s^{-1} and $k_{17} = 9 \times 10^{-11}$ cm^3 s^{-1}. The upper solid line far from the points corresponds to $k_{16} = 0$ (and $k_{17} = 0$).

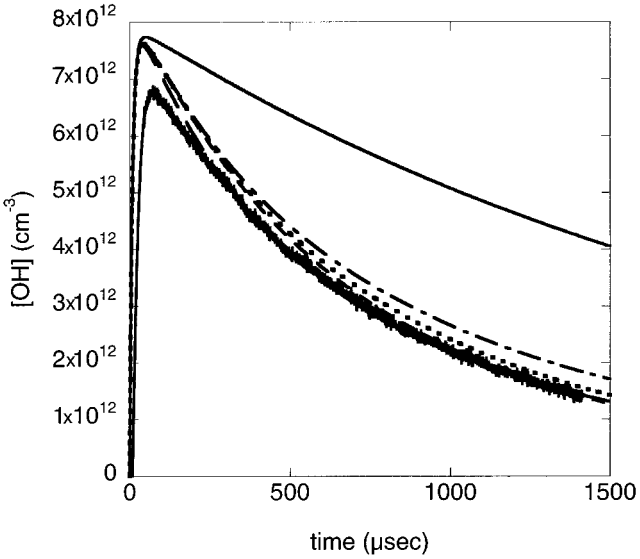

Figure 9. Time scan of [OH] with the initial partial pressure of NH_3 reduced by about a factor of 10. The initial partial pressures of NO_2 and He were the same as in Figure 7, and the excimer pulse energy and probe laser frequency were the same as Figure 8. The vertical scale is the same as in Figure 8. The experimental data are recognizable by the noise. The dotted curve uses the fitted rate constants $k_{16} = 1.8 \times 10^{-10}$ cm^3 s^{-1} and $k_{17} = 5 \times 10^{-11}$ cm^3 s^{-1}. The upper dash−dot line corresponds to $k_{16} = 1.8 \times 10^{-10}$ cm^3 s^{-1} and $k_{17} = 0$ cm^3 s^{-1}, and the lower long dash line corresponds to $k_{16} = 2.5 \times 10^{-10}$ cm^3 s^{-1} and $k_{17} = 2 \times 10^{-11}$ cm^3 s^{-1}. The dashed line between the long dash line and the dotted line corresponds to $k_{16} = 1.8 \times 10^{-10}$ cm^3 s^{-1} and $k_{17} = 9 \times 10^{-11}$ cm^3 s^{-1}. The upper solid line far from the points corresponds to $k_{16} = 0$ (and $k_{17} = 0$).

valuable to examine the time scans (see Methodology). Because of the uncertainty about whether the laser was tuned to the peak of the OH absorption line, the vertical scale of Figure 8 was

determined by adjusting $[NH_2]_0 = [OH]_0$ to get the best match of its decay for the first few hundred microseconds using the k_{16} and k_{17} values determined from the data of Figure 7. In Figure 7, the dotted line corresponds to $k_{16} = 1.8 \times 10^{-10}$ cm^3 s^{-1} and $k_{17} = 5 \times 10^{-11}$ cm^3 s^{-1}. We believe it represents the best compromise fit of the data. This value for k_{17} (5×10^{-11} cm^3 s^{-1}) is close to the value of 6×10^{-11} cm^3 s^{-1} previously assumed by Glarborg et al.[1] and Park and Lin.[8] The dashed line in Figure 7 has $k_{16} = 1.8 \times 10^{-10}$ cm^3 s^{-1} and $k_{17} = 9 \times 10^{-11}$ cm^3 s^{-1}. The dash−dot line has $k_{16} = 1.8 \times 10^{-10}$ cm^3 s^{-1} and $k_{17} = 0$. The solid line at the top, far from the data, assumes $k_{16} = 0$. Clearly k_{16} is needed. The long dash line has $k_{16} = 2 \times 10^{-10}$ cm^3 s^{-1} and $k_{17} = 2 \times 10^{-11}$ cm^3 s^{-1}. It fits the data of Figure 7 slightly better than the dotted curve but fits poorly to the data of Figure 8.

A similar choice of line types is used in Figures 8 and 9 as was used in Figure 7. In Figure 8, the model curve (a dotted line) corresponding to $k_{16} = 1.8 \times 10^{-10}$ cm^3 s^{-1} and $k_{17} = 5 \times 10^{-11}$ cm^3 s^{-1} is almost exactly superimposed on the rescaled experimental data (a thick dashed line). Figure 8 indicates that the long time behavior is most affected by the value k_{17}. The data for Figure 9 were taken without adjusting the lasers, and thus Figure 9 provides a test of the scaling of Figure 8 and the value of k_{16}. Because the concentration of the radical pool is so low that even NH_2O is reacting away slowly, reaction 17 plays almost no role in the OH decay observed in Figure 9. All models give an acceptable fit to the data in Figure 9 with the preferred model ($k_{16} = 1.8 \times 10^{-10}$ cm^3 s^{-1} and $k_{17} = 5 \times 10^{-11}$ cm^3 s^{-1}), perhaps paralleling the decay curve slightly more accurately.

We conclude that k_{16} is about $1.8(10) \times 10^{-10}$ cm^3 s^{-1} and that reaction 17 proceeds at an appreciable rate with k_{17} somewhere between 2×10^{-11} and 8×10^{-11} cm^3 s^{-1}, with our best guess of 5×10^{-11} cm^3 s^{-1}.

In all this, it is assumed that there is no reaction at room temperature between NH_2O and NO_2. Yet such a reaction seemed likely on the basis of chemical intuition. In this case, intuition proved unreliable. No effects which could be ascribable to such a reaction were observed when the system was investigated at different NO_2 concentrations. The results of varying the NO_2 concentration upon the OH decay are shown in Figure 10. Two effects are observed: the peak of the OH signal moves to shorter times when $[NO_2]$ is increased, and the [OH] signal at a very long time decreases with increasing $[NO_2]$. Both effects can be explained without bringing in a reaction between NH_2O and NO_2. The time of the maximum [OH] occurs when the rate of production of OH equals the rate of its loss. Increased NO_2 shortens the time required for OH production by reaction 14, causing the OH production rate to fall off earlier, and it shortens the time required to produce NH_2O by reaction 1b, causing the OH loss rate to peak earlier. The [OH] signal falls off more rapidly at long times with increasing $[NO_2]$ because a higher $[NO_2]$ increases the rate of reaction 18. Our modeling of the reaction predicts these changes in the OH decay curve when the NO_2 concentration is changed. Figures 9 and 10 demonstrate that, if NH_2O reacts with NO_2, the products of that reaction must react with OH with a near gas kinetic rate constant. Moreover, the yield of HNO actually increases very slightly with more NO_2. To explain this, the hypothetical products of the reaction of OH with the products of the reaction of NO_2 with NH_2O must react with OH to produce HNO with unit efficiency. The small increase of HNO with increased NO_2 is explainable by a reduction in the reaction of HNO with OH

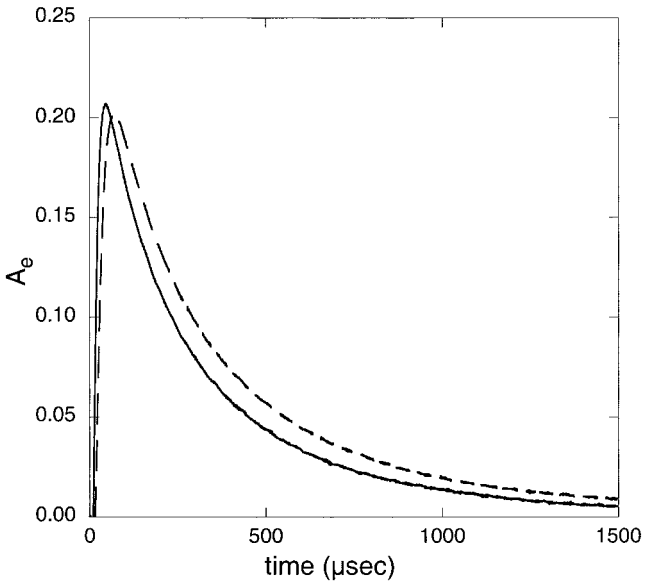

Figure 10. Effect of changing the NO_2 concentration by a factor of 2 upon the rate of OH decay. The dashed line corresponds to an NO_2 concentration of 5.9×10^{14} molecules/cm^3 and the solid line to $[NO_2] = 1.17 \times 10^{15}$ molecules/cm^3.

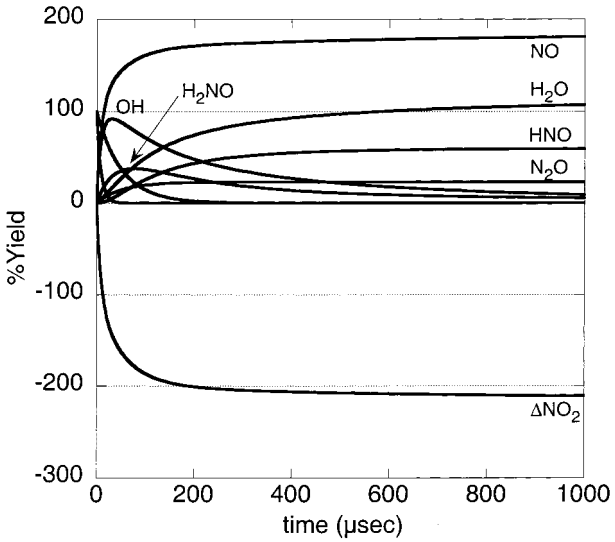

Figure 11. Concentrations of the various species resulting from the model ($k_{16} = 1.8 \times 10^{-10}$ cm^3 s^{-1} and $k_{17} = 5 \times 10^{-11}$ cm^3 s^{-1}) cast in terms of percent yield, where 100% corresponds to $[NH_2]_0$. In this model, any NH_2 and OH produced by the reaction of $O(^1D)$ with NH_3 was assumed to be produced almost instantaneously and lumped into the NH_2 produced by photolysis. The initial concentrations assumed are $[NH_2] = [H] = 4.1 \times 10^{13}$, $[NO_2] = 9.79 \times 10^{14}$, $[NH_3] = 4.4 \times 10^{14}$, and $[O(^3P)] = 3.47 \times 10^{12}$ cm^{-3}.

which removes HNO. At larger NO_2 concentrations, OH at long times is smaller because of the three body reaction (18).

Figure 11 shows the time variations of the concentrations of the various species observed and depicted in Figure 5. We believe the match between the observed concentrations and the model is excellent when the uncertainties in infrared absorption cross sections, the baseline time variations, the uncertainty about whether the laser is exactly on the IR absorption peaks, and the uncertainties in the model are considered.

The yield of N_2O from reaction 1a has been measured previously several times.[7−11] Under the conditions of our experiment, we obtain an N_2O cross section value of 3×10^{-18} cm^2, which agrees fairly well with that calculated (3.3×10^{-18} cm^2) from the HITRAN[13] value for the integrated line strength

when our measured 1/e half line widths of 214 MHz are used. The Doppler 1/e halfwidth is 143.5 MHz, which would yield a σ_0 of 4.69×10^{-18} cm^2. Our cross section (3×10^{-18} cm^2) gives a yield for N_2O of 0.27(5), and the use of HITRAN with our observed line widths (3.3×10^{-18} cm^2) gives a yield of 0.24(5). These numbers are to be compared with the results of Park and Lin[10] of 0.19 and with the last measurements[11] from Hershberger's group of 0.24. We cannot claim to have improved on previous measurements of this quantity. Our results agree well with the last from Hershberger.

Discussion

We cannot find any other way to explain either the rapid decay of OH, the appearance of HNO, or the high yield of H_2O in this system other than by the rapid reaction (16) of OH with NH_2O to produce HNO and H_2O. The necessity for the reaction (17) between HNO and OH is on less firm footing. It was introduced into the model to explain the continued excessive decay of OH at long times after the [NH_2O] becomes too low for reaction 16 to remove OH at a significant rate. The fact that reaction 17 is only marginally needed to fit the OH decay is reflected in the large uncertainty in its rate constant, k_{17}.

Acknowledgment. This work was supported by grants from the Department of Energy and the Robert A. Welch Foundation.

References and Notes

(1) Glarborg, P.; Dam-Johansen, K.; Miller, J. A. *Int. J. Chem. Kinet.* **1995**, *27*, 1207.
(2) Lyon, R. K. U.S. Patent 3, 900, 559, 1975.
(3) Brill, T. B.; Brush, P. J.; Patil, D. G. *Combust. Flame* **1993**, *92*, 178.
(4) Mebel, A. M.; Lin, M. C.; Morokuma, K.; Melius, C. F. *J. Phys. Chem.* **1995**, *99*, 6842.
(5) Atkinson, R.; Baulch, D. L.; Cox, R. A.; Hampson, R. F., Jr.; Kerr, J. A.; Rossi, M. J.; Troe, J. *J. Phys. Chem. Ref. Data* **1997**, *26*, 1329.
(6) Mebel, A. M.; Hsu, C. C.; Lin, M. C.; Morokuma, K. *J. Chem. Phys.* **1995**, *103*, 5640.
(7) Meurier, H.; Pagsberg, P.; Sillesen, A. *Chem. Phys. Lett*. **1996**, *261*, 277.
(8) Park, J.; Lin, M. C. *Int. J. Chem. Kinet.* **1996**, *28*, 879.
(9) Quandt, R. W.; Hershberger, J. F. *J. Phys. Chem*. **1996**, *100*, 9407.
(10) Park, J.; Lin, M. C. *J. Phys. Chem. A* **1997**, *101*, 2643.
(11) Lindholm, N.; Hershberger, J. F. *J. Phys. Chem. A* **1997**, *101*, 4991.
(12) Angstl, R.; Finsterhözl, H.; Funder, H.; Illig, D.; Papousek, D.; Pracna, P.; Rao, K. N.; Schrötter, H. W.; Urban, S. *J. Mol. Spectrosc.* **1985**, *114*, 454.
(13) Stephens, J. W.; Morter, C. L.; Farhat, S. K.; Glass, G. P.; Curl, R. F. *J. Phys. Chem.* **1993**, *97*, 8944.
(14) Rothman, L. S.; Rinsland, C. P.; Goldman, A.; Massie, S. T.; Edwards, D. P.; Flaud, J. M.; Perrin, A.; Camy-Peyret, C.; Dana, V.; Mandin, J. Y.; Schroeder, J.; Mccann, A.; Gamache, R. R.; Wattson, R. B.; Yoshino, K.; Chance, K. V.; Jucks, K. W.; Brown, L. R.; Nemtchinov, V.; Varanasi, P. *J. Quant. Spectrosc. Radiat. Transfer* **1998**, *60*, 665.
(15) Amano, T.; Bernath, P. F.; McKellar, A. R. W. *J. Mol. Spectrosc.* **1982**, *94*, 100.
(16) Johns, J. W. C.; McKellar, A. R. W.; Weinberger, E. *Can. J. Phys.* **1983**, *61*, 1106.
(17) Unfried, K. G.; Glass, G. P.; Curl, R. F. *Chem. Phys. Lett.* **1990**, *173*, 337.
(18) Reddington, R. L.; Olson, W. B.; Cross, P. C. *J. Chem. Phys.* **1962**, *36*, 1311.
(19) Amano, T.; Bernath, P. F.; Yamada, C.; Endo, Y.; Hirota, E. *J. Chem. Phys.* **1982**, *77*, 5284.
(20) Slagle, I. R.; Gutman, D.;. Davies, J. W.; Pilling, M. J. *J. Phys. Chem.* **1988**, 92, 2455.
(21) Schneider, W.; Moortgat, G.; Tyndall, G. S.; Burrows, J. P. *J. Photochem. Photobiol.* **1987**, *A40*, 195.
(22) Sun, F.; Hung, P.-Y.; Glass, G. P.; Curl, R. F. *Chem. Phys. Lett.* **2001**, *337*, 72.
(23) Suto, M.; Lee, L. C. *J. Chem. Phys.* **1983**, *78*, 4515.
(24) Davidson, D. F.; Chang, A. Y.; Kohse-Hoinghaus, K.; Hansen, R. K. *J. Quant. Spectrosc. Radiat. Transfer* **1989**, *42*, 267.
(25) Mikami, H.; Saito, S.; Yamamoto, S. *J. Chem. Phys.* **1991**, *94*, 3415.
(26) Johns, J. W. C.; McKellar, A. R. W. *J. Chem. Phys.* **1977**, *66*, 1217.
(27) Forster, R.; Frost, M.; Fulle, D.; Hamann, H. F.; Hippler, H.; Schlepegrell, A.; Troe, J. *J. Chem. Phys.* **1995**, *103*, 2949.
(28) Baulch, D. L.; Cobos, C. J.; Cox, R. A.; Esser, C.; Frank, P.; Just, T.; Kerr, J. A.; Pilling, M. J.; Troe, J.; Walker, R. W.; Warnatz, J. *J. Phys. Chem. Ref. Data* **1992**, *21*, 411.
(29) Adamson, J. D.; Farhat, S. K.; Morter, C. L.; Glass, G. P.; Curl, R. F.; Phillips, L. F. *J. Phys. Chem.* **1994**, *98*, 5665.
(30) Anderson, J. G.; Margitan, J. J.; Kaufman, F. *J. Chem. Phys.* **1974**, *60*, 3310.